Developments in the Built Environment 21 (2025) 100623

Contents lists available at ScienceDirect

Developments in the Built Environment

journal homepage: www.sciencedirect.com/journal/developments-in-the-built-environment

Evaluation of the flowability and non-linear rheological properties in alkali-activated concretes

Jian Zhang [a,b,c], Zhenming Li [d,e], Wentao Wang [d,e], Yaxin Tao [f], Yubo Sun [g,*], Xiangsheng Chen [a,b,c]

[a] Key Laboratory of Coastal Urban Resilient Infrastructures (Shenzhen University), Ministry of Education, Shenzhen, 518060, China
[b] State Key Laboratory of Intelligent Geotechnics and Tunnelling, Shenzhen University, Shenzhen, 518060, China
[c] College of Civil and Transportation Engineering, Shenzhen University, Shenzhen, 518060, China
[d] School of Civil and Environmental Engineering, Harbin Institute of Technology, 518055, Shenzhen, China
[e] Guangdong Provincial Key Laboratory of Intelligent and Resilient Structures for Civil Engineering, Harbin Institute of Technology, 518055, Shenzhen, China
[f] Institute for Building Materials, ETH Zurich, 8093, Zurich, Switzerland
[g] Department of Civil and Environmental Engineering, The Hong Kong Polytechnic University, 999077, China

ARTICLE INFO

Keywords:
Alkali-activated slag concrete
Rheological behavior
Non-linearity
Shear thinning
Shear thickening

ABSTRACT

Alkali-activated materials (AAMs) emerge as a sustainable alternative to Portland cement binders. Despite their potential, the rheological properties of alkali-activated concrete, particularly their non-linear behaviors, remain underexplored. To bridge this gap, a comparative study was conducted to examine the flow characteristics and shear thinning/thickening tendencies of alkali-activated slag (AAS) concrete. The research began with a detailed evaluation of the setting times of AAS mixtures, optimizing activator compositions to identify formulations suitable for concrete productions. Employing the Bingham and Herschel-Bulkley models, it was observed that AAS concrete with a lower silicate modulus (Ms) predominantly exhibited shear-thinning behavior. As the Ms increased, a shift toward shear-thickening behavior occurred, becoming more pronounced with higher concentrations of alkaline compounds in the activators. Furthermore, the fresh properties of AAS concrete significantly improved with increased alkali dosages in the activators, resulting in reduced dynamic yield stress and plastic viscosity, along with enhanced workability retention over time.

1. Introduction

Alkali-activated materials (AAMs) are innovative binders that utilize industrial by-products, combined with alkaline activators (Provis and Van Deventer, 2013; Ren et al., 2025). They present a sustainable alternative to traditional Portland cement (PC), addressing both environmental concerns and material performance (Juenger et al., 2011; Ma et al., 2025; Sivakrishna et al., 2020). By utilizing industrial by-products and waste materials, as well as avoiding the limestone calcination for PC production, AAMs benefit in both waste reduction and decrease greenhouse gas emissions (van Deventer et al., 2021; Thwe et al., 2021; Zhang et al., 2025). Previous works have revealed substantial reductions in CO_2 emissions and environmental impact compared to conventional PC (Tsiropoulos et al., 2020; Vieira et al., 2021). On top of that, AAMs have demonstrated impressive performances, including high compressive strength, durability, and resistance to aggressive environments (Duxson and Brice, 2010; Provis, 2014; Krivenko, 2017), exhibiting great potential as an alternative binder to be applied in the construction sector.

Nevertheless, the application of AAM concrete in construction has been quite restricted due to challenges with workability issues. These issues have interfered with mixing, transportation, casting, and compacting operations. Previous studies have highlighted the rapid degradation of workability in AAM mixtures, especially those with a high dosage of silicate in the activator (Alrefaei et al., 2020) (Palacios et al., 2008) (Sun et al., 2022a). Moreover, previous studies suggested that conventional superplasticizers for PC materials may not provide a fluidizing effect in AAMs, especially with the presence of silicate in activators (Criado et al., 2009) (Sun et al., 2024a). The appropriate rheology control in AAMs still remains problematic.

Rheology of PC concrete has been extensively studied for decades.

This article is part of a special issue entitled: Upcycling of Waste published in Developments in the Built Environment.

* Corresponding author.
E-mail address: yubo.sun@polyu.edu.hk (Y. Sun).

https://doi.org/10.1016/j.dibe.2025.100623
Received 2 October 2024; Received in revised form 6 January 2025; Accepted 7 February 2025
Available online 10 February 2025

The Bingham model (Tattersall and Banfill, 1983; Yang et al., 2025) has been proposed to describe rheological properties through a simple linear fitting, which has been validated for broad applications. To meet the self-compacting demand, modern concrete formulations incorporate various admixtures and fine fillers to reduce the yield stress while avoiding segregation (Okamura and Ouchi, 2003) (De Schutter et al., 2008) (Zhang et al., 2024a). Consequently, recent scholars have reported deviations between testing and Bingham fitting results, underlining the non-linear relationship between shear stress and shear rate in the concrete (Feys et al., 2009) (Wang et al., 2025) (Wang et al., 2022). Modified models have been proposed to identify the shear thinning/thickening behaviors, assisting in better expressing the non-linear relationship (De Larrard et al., 1998) (Feys et al., 2008). The non-linearity of concrete is of great interest in practical applications. Yahia (2011) proposed that the shear thinning behavior might improve the concrete stability after casting. On the contrary, shear thickening appears to be more tricky as the energy required is exponentially increased to accelerate the flow. However, such behavior is sometimes neglected since concrete rheological tests are performed in the 'linear' region with lower shear rates (Barnes, 1989). In that case, the actual shear stress regarding operations with high shear rates (e.g. concrete mixing and pumping) might be way higher than predicted values, which could possibly result in critical damage to the equipment (Feys et al., 2009). Therefore, extra attention should be paid to percept and properly control shear thickening behaviors in the fresh concrete.

In contrast to PC binders, additional chemical substances in either liquid or solid forms are incorporated in AAMs to facilitate the dissolution of precursors due to their limited reactivity in water (Provis and Van Deventer, 2013; Krivenko, 2017). Sodium hydroxide and silicate are recognized as the most widely used alkaline activators in AAMs (Provis and Van Deventer, 2013). Activators are typically defined by their sodium oxide (Na_2O) content relative to the weight of precursors and their silicate modulus (Ms), denoting the molar ratio of SiO_2 to Na_2O. Variations in both factors will lead to significant impacts on the property of AAMs (Aydın and Baradan, 2014). Reports indicate that adding alkaline substances to the activator enhances viscosity while minimizing colloidal interactions in fresh AAMs. (Alnahhal et al., 2021) (Gong et al., 2024). Moreover, distinctive particle interactions and microstructural features have been observed in alkali-activated slag (AAS) mixtures as compared to conventional PC materials (Sun et al., 2022b) (Sun et al., 2023). Regarding the non-linear behaviors, Puertas et al. (2014) reported linear rheological behaviors of AAS pastes prepared with NaOH and Na_2CO_3 activators. Palacios et al. (2008) noted that AAS paste prepared with sodium silicate conforms more closely to the non-linear Herschel-Bulkley model. Dai et al. (2022) observed a shift from shear thinning to shear thickening behavior in NaOH-activated slag pastes as the activator concentration increased. However, the rheological properties of AAM concrete remain largely unexplored, while only a few attempts have been made by adopting the linear Bingham model to express stress-speed relationships (Puertas et al., 2018) (Zhang et al., 2023) (Laskar and Bhattacharjee, 2011). Existing knowledge does not yet fully explain the rheological properties of AAM concrete.

The current work aims to thoroughly investigate the flowability and non-linear rheological characteristics of alkali-activated concrete. The initial step involved a comprehensive assessment of the setting time of AAS mixtures by modifying activator compositions to identify mixtures suitable for practical concrete production. The rheology of AAS concretes were analyzed using Bingham and Herschel-Bulkley models, focusing on variations in Na_2O content and Ms in the activator to explore shear thinning and thickening behaviors. Comprehensive discussions were provided to offer insights into the non-linearity compared to conventional PC concretes. In addition, static yield stress and workability were tested over time to evaluate time-dependent rheological behaviors. These results can inform the production of alkali-activated concrete with ideal rheological properties.

2. Materials and method

2.1. Raw materials

Commercial blast furnace slag (BFS) was used in this study as the aluminosilicate precursor, with a specific gravity of 2.89. The precursor particle fineness was detected with laser diffraction, as displayed in Fig. 1 (a), and the median size (d_{50}) of BFS particles is 8.28 μm. The surface texture and morphology of precursor grains were examined using a scanning electron microscope (SEM, JEOL JSM-IT800) in secondary electron (SE) mode at 1000 $\times$ magnification, as illustrated in Fig. 1 (b). In addition, the chemical composition of precursors was characterized using X-ray fluorescence (XRF), and the results detailed in Table 1.

In this study, hybrid activators made from sodium hydroxide and sodium silicate were used. The sodium hydroxide (anhydrous pearls, >99% purity) and the sodium silicate solution (comprising 30% SiO_2, and 15% Na_2O) were received from Aladdin Co., Ltd. In addition, locally sourced silica sand and gravels were utilized as aggregates in the production of AAS concrete. The specific physical properties and water absorption rates of aggregates in different particle fractions are detailed in Table 2. It should be noted that the aggregates were oven-dried at 105 °C for 24 h prior to mixing.

2.2. Mixture proportions

2.2.1. Mixture screening based on setting features

AAS mixtures were characterized by inherently shorter setting time compared to PC binders, and thereby obstructing their practical application (Palacios et al., 2021) (Sun et al., 2024b). At the initial stage of this study, a preliminary screening on AAS paste was carried out to ensure a sufficient setting time in view of concrete productions in practice. The Na_2O content and Ms of the activator solutions, as previously indicated, were modified to evaluate their impact on the rheological properties of AAS. Na_2O content applied in this study was varied from 2% to 6%, as higher dosages resulted in extremely rapid setting in trial mixes, while lower values are insufficient for alkali-activation reactions (Wang et al., 1994). The Ms value varied from 0 to 2, constrained by the composition of the commercial sodium silicate solution used in this study. On top of that, the water-to-binder (w/b) ratio was consistently maintained at 0.45 across all AAS mixtures to ensure appropriate consistency for the subsequent preparation of AAS concrete. Details of 50 mixtures of AAS paste are presented in Table 3, for assessment on the setting time (section 2.4.1).

2.2.2. Mix design of AAS concrete

AAS pastes with an initial setting time exceeding 60 min were chosen for concrete upscaling studies. Table 4 presents the mix design for AAS concretes, maintaining a constant precursor dosage of 400 kg/m^3 across all mixes. Based on the screening results, activators were prepared with a Na_2O content ranging from 3% to 6%, and Ms values between 0.25 and 1.25. The w/b ratio was kept at 0.45 across various mixtures. Extra water content was incorporated to offset the amount absorbed by the dried aggregates, as determined by the absorption rates outlined in Table 2, along with the water content present in the activator solutions. Alkaline solutions were prepared by intermixing sodium hydroxide and sodium silicate with tap water to achieve the desired composition outlined in Table 4. The prepared activators were covered to prevent moisture loss and were cooled to ambient temperature 24 h before use. By adjusting the alkali dosages in the activator, changes in the unit volume of AAS concrete were balanced by modifying the aggregate content. The aggregate gradation was designed to fit between the A16 and B16 curves according to DIN 1045-2 (Sun et al., 2024a).

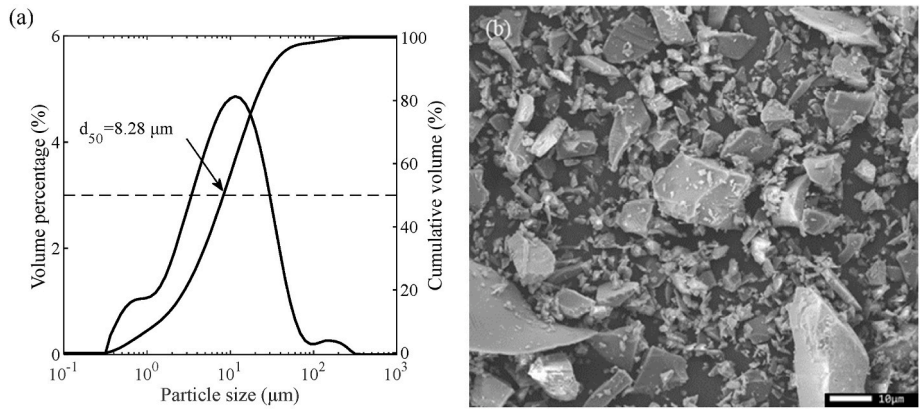

Fig. 1. (a) Particle size distribution of BFS precursors by laser diffraction; (b) Surface morphology of BFS precursors by SEM (1000 × magnification).

Table 1
Chemical composition of BFS precursors (wt.%).

CaO	SiO_2	Al_2O_3	MgO	Na_2O	K_2O	SO_3	TiO_2	Fe_2O_3	MnO	ZrO_2	LOI [a]	Other
40.90	30.10	13.70	9.07	0.65	0.60	2.40	1.35	0.36	0.35	0.14	0.08	0.38

Table 2
Water absorption and specific gravity of aggregates.

Aggregate	Fine	Coarse 1	Coarse 2
Particle fractions (mm)	0–4	2–8	8–16
Water absorption (%)	0.33	0.65	0.55
Specific gravity	2.65	2.64	2.67

2.3. Sample preparation

Investigations on the initial setting time were conducted at the paste level. AAS pastes were prepared using a handheld mixer, following the same mixing protocol as for AAS concretes detailed below. The fresh AAS pastes were then collected for setting time tests. AAS concretes were produced in 30-L per batch using a Gustav Eirich SKG1 mixer. The solid ingredients (precursor, sand, and gravels) were initially dry-mixed for 120 s to achieve uniformity. Subsequently, the liquid activators were gradually added over 30 s and mixed for an additional 3 min. The freshly prepared AAS concrete was then used for rheological and slump tests.

2.4. Testing program

2.4.1. Setting time

The initial setting time for various AAS paste mixtures was determined using an automatic Vicat needle apparatus in accordance with EN 196-3 (Ruiz-Sánchez et al., 2019). The results presented for each mixture was calculated as the average from two replicate samples.

Table 3
AAS paste mix design for the preliminary screening on setting time.

Mixtures (w/b = 0.45)		Silicate modulus (Ms)									
		0	0.125	0.25	0.5	0.75	1.0	1.25	1.5	1.75	2.0
Na_2O content (%)	2	P2.1	P2.2	P2.3	P2.4	P2.5	P2.6	P2.7	P2.8	P2.9	P2.10
	3	P3.1	P3.2	P3.3	P3.4	P3.5	P3.6	P3.7	P3.8	P3.9	P3.10
	4	P4.1	P4.2	P4.3	P4.4	P4.5	P4.6	P4.7	P4.8	P4.9	P4.10
	5	P5.1	P5.2	P5.3	P5.4	P5.5	P5.6	P5.7	P5.8	P5.9	P5.10
	6	P6.1	P6.2	P6.3	P6.4	P6.5	P6.6	P6.7	P6.8	P6.9	P6.10

Table 4
Mix design of AAS concretes.

Mix	BFS precursor (kg/m^3)	Activator					w/b [a]	Aggregates (kg/m^3)		
		Sodium hydroxide (kg/m^3)	Sodium silicate (kg/m^3)	Na_2O	Ms	Extra water (kg/m^3)		0–4 mm	2–8 mm	8–16 mm
C3.3	400	13.55	10.00	3%	0.25	191.22	0.45	701	482	572
C3.4		11.61	20.00		0.5	186.86		701	482	572
C3.5		9.68	30.00		0.75	182.51		700	481	571
C3.6		7.74	40.00		1.0	178.15		699	480	570
C3.7		5.81	50.00		1.25	173.79		698	480	570
C4.3		18.06	13.33	4%	0.25	191.98		692	476	565
C4.4		15.48	26.67		0.5	186.15		689	474	563
C4.5		12.90	40.00		0.75	180.32		686	472	560
C5.4		19.35	33.33	5%	0.5	185.52		685	471	559
C5.5		16.13	50.00		0.75	178.26		683	470	558
C6.4		23.23	40.00	6%	0.5	184.85		677	465	553

[a] Calculated by dividing the total water (from both the aqueous activator and any additional water) by the combined weight of the precursor and solid activators.

2.4.2. Rheology of AAS concrete

The testing procedures for assessing the fresh properties of AAS concretes are outlined in Fig. 2. Rheological properties of AAS concretes were assessed using a coaxial rheometer fitted with a cylinder container (ICAR Plus, Germann Instruments). Initially, 20 L of the fresh concrete were placed into a cylindrical container with a depth of 390 mm and an inner diameter of 286 mm, while the remaining concrete was used for slump testing. The concrete in the container was remixed for 1 min with a handheld concrete mixer to erase the thixotropic build-up while achieving a consistent reference state (Sun et al., 2022b). A rheometer vane with 4 blades, measuring 130 mm in both diameter and height, was then inserted. The concrete was allowed to rest to release the undissipated energy before proceeding with further tests.

Flow curve tests commenced 10 min after the initial contact between the solid and liquid ingredients. A high initial shear rate of 0.6 rps was applied to eliminate the build-up during rest, followed by shear steps with both increasing and decreasing rotational speeds. As shown in Fig. 3, the rotational speed varied between 0.05 and 0.6 rps, with a stepwise variation of 0.05 rps. The shear at each speed was maintained for 10 s, and the equilibrium state was determined by averaging the torque over the last 2 s. Flow curves were depicted using the descending sections in the torque-rotational speed profiles, and rheological parameters were determined by fitting with Bingham (Eq. (1) (Tattersall and Banfill, 1983)) and Herschel-Bulkley models (Eq. (2) (Feys et al., 2008)). Further, the torque-rotational speed values were converted into fundamental rheological parameters by using Reiner-Riwlin equations (Eqs. (3) and (4) (Feys et al., 2013)) and their extensions for the Herschel-Bulkley model (Eqs. (5) and (6) (Feys et al., 2008) (Heirman et al., 2008)). The non-linear rheological behavior is reflected by the flow index n ($n < 1$ for shear thinning, $n > 1$ for shear thickening, and $n = 1$ aligns with the linear Bingham model (Sun et al., 2024b)).

$$\tau = \tau_0 + \mu \bullet \dot{\gamma} \tag{1}$$

$$\tau = \tau_0 + \mathrm{K} \bullet \dot{\gamma}^n \tag{2}$$

$$\tau_0 = \frac{\left(\frac{1}{R_1^2} - \frac{1}{R_2^2}\right)}{4\pi h \ln\left(\frac{R_2}{R_1}\right)} G_B \tag{3}$$

$$\mu = \frac{\left(\frac{1}{R_1^2} - \frac{1}{R_2^2}\right)}{8\pi^2 h} H_B \tag{4}$$

$$\tau_0 = \frac{\left(\frac{1}{R_1^2} - \frac{1}{R_2^2}\right)}{4\pi h \ln\left(\frac{R_2}{R_1}\right)} G_{HB} \tag{5}$$

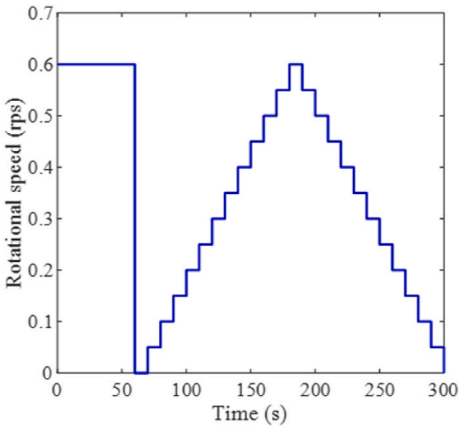

Fig. 3. Shear protocol used for flow curve tests.

$$K = \frac{\left(\frac{1}{R_1^{2/n}} - \frac{1}{R_2^{2/n}}\right)^n}{2^{2n+1}\pi^{n+1}h} H_{HB} \bullet n^n \tag{6}$$

where τ is the shear stress (Pa), τ_0 is the dynamic yield stress (Pa), μ is the plastic viscosity (Pa • s), $\dot{\gamma}$ is the shear rate (1/s), K represents the consistency factor (Pa • s^n), n represents the flow index (−), R_1 is the radius of the vane (m), R_2 is the radius of the concrete container (m), G_B represents the intercept of the descending flow curve in the Bingham model (Nm), H_B is the slope of the fitted curve in the Bingham model (Nm·s), G_{HB} represents the intercept of descending flow curves in the Herschel-Bulkley model (Nm), and H_{HB} represents the slope of fitted curves in the Herschel-Bulkley model (Nm·s).

Meanwhile, stress growth tests were carried out also 10 min after the first contact between solid and liquid ingredients, on new batches of mixtures to prevent the effects of shear history. To measure the static yield stress, a fixed rotational speed of 0.025 rps was sustained for 60 s. The static yield stress was determined from the peak torque recorded, using Eq. (7) (Koehler and Fowler, 2004), which represents the energy needed to trigger the flow from a static state. Stress growth tests were repeated every 15 min till 1 h to evaluate the structural build-up process in AAS concrete, with the initial measurement was marked as '0 min'. After each test, the rheometer vane was removed, and the fresh concrete was covered with a plastic sheet to prevent moisture loss, allowing for rest. Before each scheduled testing interval, the AAS concrete was subjected to a 1-min remixing with a handheld concrete mixer and then allowed to rest for another minute (Puertas et al., 2018). The rheological tests presented in this study were performed on two replicate AAS concretes to ensure repeatability.

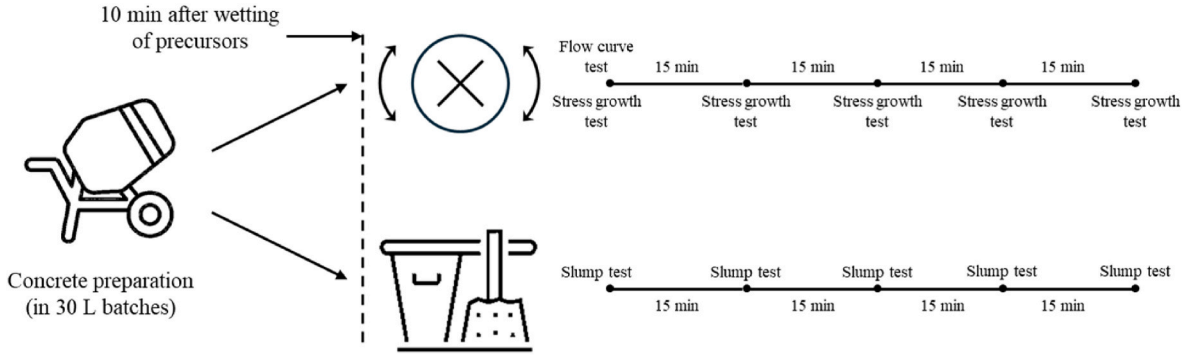

Fig. 2. Flowchart outlining the testing procedures for evaluating the fresh properties of AAS concretes.

$$\tau_s = \frac{2T}{\pi d_v^{\,3}\left(\frac{h_v}{d_v}+\frac{1}{3}\right)} \quad (7)$$

where τ_s represents the static yield stress (Pa), T represents the maximum torque (Nm), d_v represents the vane's diameter (m), and h_v represents the vane's height (m).

2.4.3. Workability retention of AAS concrete

Slump tests were in parallel conducted every 15 min according to EN 12350-2 with an Abrams cone to evaluate the workability retention of AAS concrete (Sun et al., 2022c). The concrete for slump tests was also remixed for 1 min before target testing ages (Puertas et al., 2018). To mitigate the influence of potential losses of mortar and paste, the fresh mixture attached to the surface of testing devices was carefully recollected into the container. Results presented in the current study were presented as the average of two tests.

3. Results and discussion

3.1. Mixture screening based on setting features

Results of mixture screening based on the setting features of AAS pastes are shown in Fig. 4. The mesh surface representing the initial setting time as a function of Ms and Na_2O content in the activator is derived by piecewise linear interpolations between two adjacent data points (Table 3). Results have illustrated that the initial setting time gradually decreased with an elevated Na_2O content given a certain Ms in the activator. It can be inferred that the increase in alkalinity has considerably facilitated the initial dissolution of precursors, resulting in a rapid initial setting. By contrast, a non-linear relationship was detected between Ms and the setting time. With a fixed Na_2O content, the initial setting time was first extended but drastically declined along with the increases in Ms. In specific, AAS with Ms of 0.75 exhibited the longest setting times among all mixtures with 2% Na_2O content. Moreover, it was noted that the Ms values resulted in the longest setting time shifted towards lower Ms values (around 0.5) with further increases in Na_2O content in the activator, as denoted with the dashed arrow in Fig. 4 (b). This shift may be attributed to the unique stiffening mechanism resulting from modifications in activator compositions (Sun et al., 2023) (Palacios et al., 2021). In turn, a triangle zone was observed as presented by the warm colors in Fig. 4 (b), indicating AAS mixtures with an apparently longer setting time over other mix designs.

According to EN 197-1, the minimum initial setting time for cement should range from 45 to 75 min, depending on its strength classification (Luukkonen et al., 2018). In this study, a threshold of 60 min was established for subsequent tests, and the chosen mixtures were used as paste components in the AAS concrete mix design (see Table 4). Further, it was found that AAS pastes with 2% Na_2O exhibited very limited strength development after 24 h that the hardened Vicat apparatus samples could be manually crushed while demolding. Accordingly, they were excluded from subsequent studies on AAS concrete as well.

3.2. Non-linear rheological behaviors

Fig. 5 presents the ramp-down portions in torque-rotational speed curves of AAS concretes with different activator compositions. It was observed that flow curves shifted downwards with the increase in either Ms or Na_2O content. The rheological parameters were determined with the method described in Section 2.4.2 to characterize the dynamic flow of AAS concrete, as illustrated in Table 5. Using the linear Bingham model, C3.3 exhibited the highest dynamic yield stress and plastic viscosity. However, both parameters significantly decreased as Ms

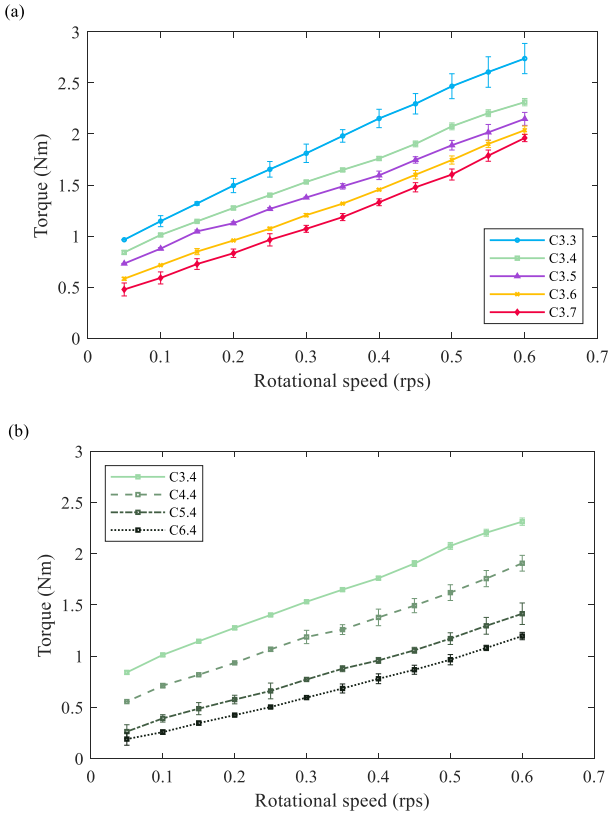

Fig. 5. Results of flow curve tests (a) Flow curves of AAS concretes with 3% Na_2O; (b) Flow curves of AAS concretes with Ms0.5.

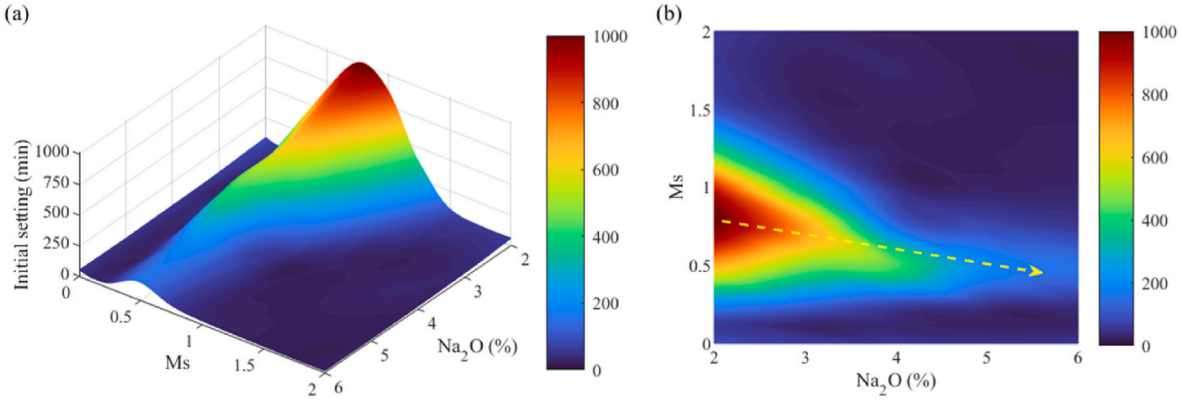

Fig. 4. Initial setting time of AAS paste (w/b = 0.45) versus Ms and Na_2O content (%) in activators (a) 3D view; (b) Top view.

increased. Specifically, the dynamic yield stress of C3.7 dropped by 63.2% compared to C3.3, highlighting the fluidizing effect of silicate species in the activators (Alonso et al., 2017). It is noteworthy that the plastic viscosity of 3% Na_2O concrete mixtures was first reduced with the increase of Ms, but slightly improved in C3.6 and C3.7. Meanwhile, the increase of Na_2O content in the activator resulted in similar reductions of both rheological parameters This might be ascribed to higher liquid content in the fresh concrete by improving the alkali dosage, in particular the sodium silicate, leading to better dispersion between solid particles (Puertas et al., 2018).

Typical flow curves of C3.3 and C3.7 fitted with Bingham and Herschel-Bulkley models are plotted in Fig. 6. In both cases, the Bingham fitting curve was found more deviated from the flow curve obtained from the rheological test, where an explicit non-linearity was identified instead. Hence, the Herschel-Bulkley model was further adopted to accurately assess the non-linear rheological behavior in AAS concrete. As listed in Table 5, progressive growth of the flow index from 0.92 to 1.23 was detected in 3% Na_2O AAS concretes with the increase of Ms, indicating a transition between shear thinning and shear thickening behaviors (Yahia, 2011). Similar trends have been found in 4% Na_2O mixtures. In addition, the shear thickening of AAS concrete became more pronounced by improving the Na_2O content in the activator, and the maximum flow index of 1.22 occurred in C6.4 among Ms0.5 mixtures.

Meanwhile, an almost linear rheological behavior was detected in C3.5 and C4.4, with the flow index of 1.01 and 1.02, respectively. Bingham and Herschel-Bulkley models have resulted in equivalent performances in C3.5 and C4.4 with nearly identical rheological parameters. However, the Herschel-Bulkley model exhibited a better fitting with greater R^2 over the other as the non-linearity became more evident, especially in mixtures with higher alkali dosages. Results reveal that both the yield stress and consistency factor were reduced with the increase of Ms and Na_2O content, indicating a more fluid flow of AAS concrete. Moreover, it is noticed that the viscosity of AAS concrete (denoted with the consistency factor in the Herschel-Bulkley model (Feys et al., 2008)) gradually declined with the increase of Ms. Instead, the inverse increment of plastic viscosity from C3.5 to C3.7 by applying the Bingham model disappeared. This could be attributed to the non-linearity of the dynamic flow. In that case, the viscous behavior in AAS concrete was overestimated due to shear thickening. On top of that, it has been also indicated that the shear stress could be underestimated with the Bingham model in low shear rate regions (Feys et al., 2007). Negative shear stress has been reported in some extreme cases, which is physically unrealistic in practice (De Larrard et al., 1998) (Heirman et al., 2008). Results above further illustrate that the Herschel-Bulkley model could better describe the rheological behavior of AAS concrete over the Bingham model, in particular while high dosages of alkaline activators are applied.

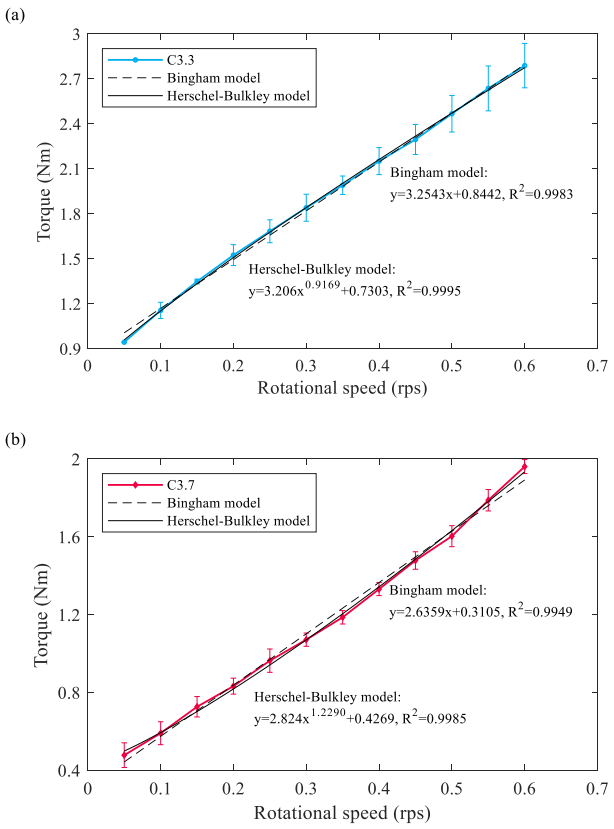

Fig. 6. Flow curves fitting of AAS concretes (a) Flow curve of C3.3; (b) Flow curve of C3.7.

3.3. Structuration and workability retention

Stress growth tests using a rheometer and slump tests were conducted in parallel every 15 min until 1 h to monitor the structuration and workability retention in AAS concrete. The effect of concrete thixotropy was eliminated by the 1-min remixing process before each testing age.

As shown in Fig. 7 (a), C3.3 exhibited the highest static yield stress over time among 3% Na_2O mixtures. A very steep increase was detected between 15 and 30 min in C3.3, and it was no longer possible to remix and conduct further tests at later ages. Meanwhile, the static yield stress in AAS concrete gradually declined with an elevated Ms, indicating the fluidizing effects of sodium silicate activators (Alonso et al., 2017). The stress evolution curves gradually stabilized from C3.4 to C3.7 over time. This may be linked to the extended induction period, during which the activation reaction proceeded at a relatively slow pace. Meanwhile, the reversible accumulation was progressively diminished due to the applied remixing shear steps. Thereby, these mixtures exhibited a

Table 5
Results of flow curve fitting with the Bingham and Herschel-Bulkley models.

Mix	Bingham model			Herschel-Bulkley model			
	Dynamic yield stress (Pa)	Plastic viscosity (Pa·s)	R^2	Dynamic yield stress (Pa)	Consistency factor (Pa·s^n)	Flow index	R^2
C3.3	129.56	63.69	0.9970	114.72	78.22	0.92	0.9988
C3.4	112.69	52.46	0.9986	111.11	54.10	0.98	0.9986
C3.5	96.09	49.90	0.9980	97.11	48.87	1.01	0.9980
C3.6	66.88	52.01	0.9978	78.70	40.01	1.14	0.9993
C3.7	47.72	52.34	0.9949	65.60	34.42	1.23	0.9985
C4.3	111.92	59.67	0.9990	105.24	66.68	0.94	0.9993
C4.4	70.29	46.77	0.9976	71.74	45.27	1.02	0.9976
C4.5	57.09	42.39	0.9983	62.55	36.81	1.08	0.9987
C5.4	25.68	40.25	0.9979	31.33	34.50	1.08	0.9984
C5.5	16.67	38.40	0.9969	25.80	29.18	1.15	0.9984
C6.4	10.30	36.00	0.9962	22.13	24.14	1.22	0.9995

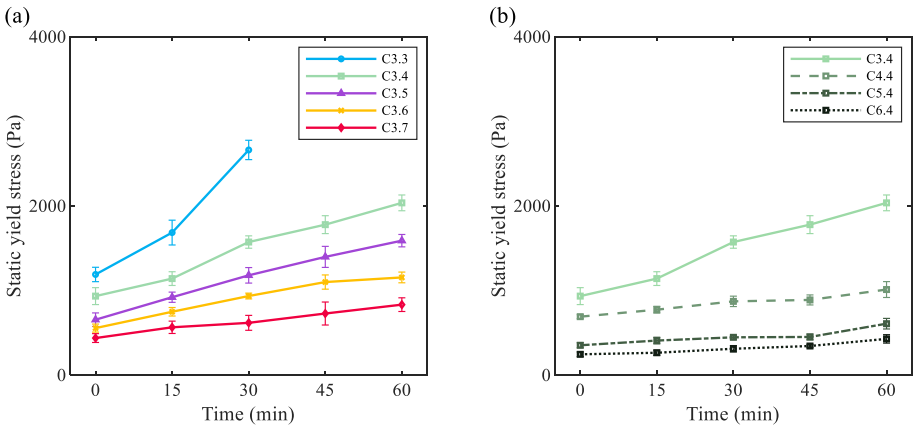

Fig. 7. Results of stress growth test as a function of time (a) Static yield stress of AAS concretes with 3% Na_2O; (b) Static yield stress of AAS concretes with Ms0.5.

limited structuration in the first hour compared to C3.3. Similarly, previous studies have also reported fluidity recovery by extending the mixing time and applying extra shear energy in silicate-activated AAS mixtures (Puertas et al., 2018; Palacios et al., 2021; Palacios and Puertas, 2011).

Regarding Ms0.5 mixtures (Fig. 7 (b)), the static yield stress was found to decrease with a higher Na_2O content. From the mix design point of view, extra sodium silicate was introduced into the AAS concrete to keep a constant Ms while increasing the Na_2O content, leading to a more dispersed system by improving the liquid fraction. As the solid grains are more dispersed from each other (Okamura and Ouchi, 1999), more reaction products are needed to achieve comparable interparticle interactions and thus improve the stiffness of fresh mixtures. Therefore, AAS concretes with higher alkali dosages exhibited a slower structural build-up progress compared to other mixtures (Fig. 7).

Fig. 8 shows the slump values of AAS concrete over time. The initial slump increased with higher Ms and Na_2O content, while the rate of slump loss decreased slightly with increased alkali dosages. The highest initial slump value was detected in C6.4, where an S5 consistency class (according to EN 206) has been achieved. In the meantime, C6.4 also exhibited good workability retention that the slump maintained more than 200 mm after 1 h.

Moreover, the static yield stress and slump results presented above exhibited similar evolutionary trends. A correlation likely exists, as both parameters describe the onset of the dynamic concrete flow from a static state. Previous rheological studies have identified the correlations between yield stress and slump values in PC concrete (Domone et al., 1999) (Ferraris and De Larrard, 1998). However, relevant information on the application of AAS concrete has been seldom reported since the rheological data is very limited in the present literature to date. Results obtained from this study are plotted in Fig. 9. An exponential relationship with an R^2 of 0.89 has been established between the static yield stress and slump of AAS concrete. The result further explores the feasibility of predicting AAS concrete yield stress through a simple slump test, whereas more relevant data is needed to establish the relationship with better accuracy.

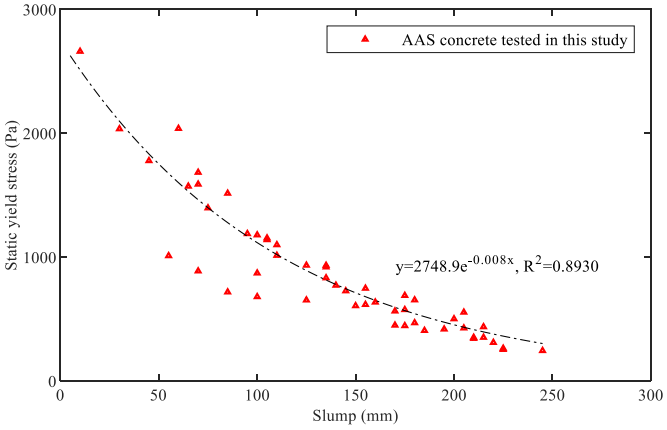

Fig. 9. Correlations between the static yield stress and slump values of AAS concretes.

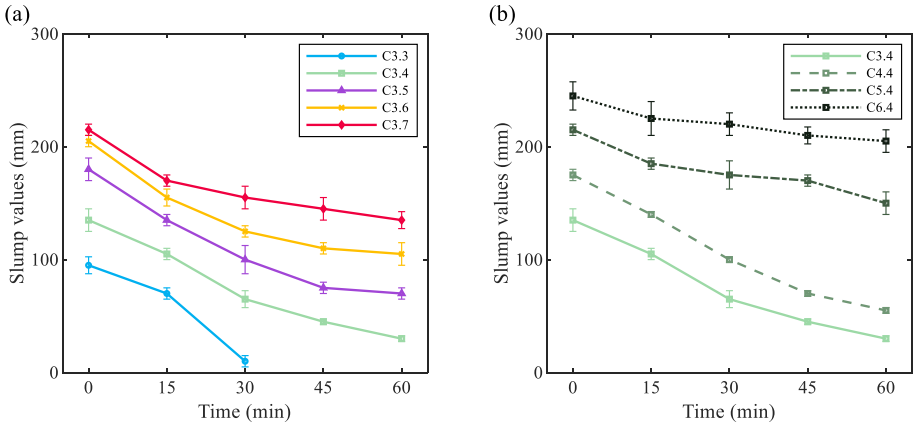

Fig. 8. Results of slump tests as a function of time (a) Slump values of AAS concretes with 3% Na_2O; (b) Slump values of AAS concretes with Ms0.5.

3.4. Discussion

The origin of non-linearity in dynamic flows of concrete has been addressed in previous studies using PC binders. Several studies have explained the shear thinning and thickening through the transition between ordering and disordering states of particles in suspensions (Feys et al., 2009) (Houst et al., 2008). In these systems, hydrodynamic forces induced by external shear energy applied are competing with the interparticle Brownian force (Rastogi et al., 1996) (Feys et al., 2009), and thus the non-linear behavior is driven by the balance between interparticle attractions and repulsions (Yahia, 2011). Shear thinning occurs as the hydrodynamic force exceeds the interparticle attractive force under dynamic flows to disperse the particles, leading to a shear-induced ordering of the system (Feys et al., 2008) (Zhang et al., 2024b). As illustrated in Fig. 6 (a), C3.3 with the lowest Ms behaved shear thinning at low rotational speed regions, while the torque almost linearly increased with higher rotational speeds. It can be inferred that the randomly packed particles in AAS concrete initiated their relative motions with the increase in shear rate, until reaching an ordering state to maintain the dynamic flow in equilibrium. In that case, the internal shearing takes place only between layers of particles and the interstitial fluid against the flow at higher shear rates (Feys et al., 2009), where no further shear thinning was detected.

On the other hand, there exists a competition between the inherent interparticle interactions and external shear applied under dynamic flow conditions (Melrose and Ball, 2004a). Shear thickening usually occurs with an increase in shear rate because hydrodynamic forces become dominant, overcoming interparticle electrostatic repulsion and wrecking the dynamic equilibrium. (Maranzano and Wagner, 2001a) (Maranzano and Wagner, 2001b). In other words, the interparticle repulsive forces cannot instantly relieve hydrodynamic forces induced by the increase of external shear energy applied, and thus the adjacent solid grains are forced to approach closer from each other until reaching the new equilibrium at higher energy levels (Melrose and Ball, 2004b). In turn, solid particles including undissolved binders and precipitates of early reaction products are temporarily compressed into clusters, in which the solid grains nearby are freely accessible depending on the shear energy applied. (Feys et al., 2009). Further, solid grains tend to accumulate in clusters, obstructing the flow path as the shear energy propagates from high to low shear rate areas. This can enhance interparticle interactions, increasing apparent viscosity and resulting in more pronounced shear thickening behavior (Egres and Wagner, 2005).

By incorporating alkaline compounds in to the activator solutions, AAMs inherently exhibit a distinctive viscous effect in interparticle fluids compared to PC materials (Alnahhal et al., 2021) (Favier et al., 2014). Moreover, higher Ms in the activator may lead to a more viscous interstitial fluid (Alnahhal et al., 2021), which in turn easily entrap the free solid particles in the cluster along the shear direction. Apart from that, a few previous works have further illustrated that the silicate species in activators may provide nucleation sites for primary reaction products (Hubler et al., 2011), resulting in the rapid structural build-up at the early stage (Sun et al., 2023) (Zhang et al., 2022) (Gebregziabiher et al., 2015). As the Ms content in the activator increased, the mechanisms described earlier became more prominent, enhancing the shear thickening behavior (Maranzano and Wagner, 2001b), as evidenced by the rises in flow index in Table 5. An apparent shear thickening was observed in C3.7 (Fig. 6 (b)) that the flow curve progressively became steeper in high rotational speed regions.

In addition, the shear thickening is also related to microstructural configurations in the system. Barnes (1989) suggested that shear thickening is not featured in typical flocculated systems. This is further corroborated by Feys et al. (2009), who found that conventional concretes with more flocculated particles show less shear thickening compared to self-compacting concrete, where fine particles are dispersed using admixtures. In AAS mixtures, previous studies have revealed the similar effects of silicate species in activators to disperse slag grains (Sun et al., 2022b), resulting in a less flocculated microstructural feature in the system. Accordingly, the shear thickening was gradually intensified in AAS concretes with an elevated Ms.

Nevertheless, the contribution of aggregates is significant and should not be overlooked. In this study, AAS concretes were prepared with a fixed precursor content, whereas the variations of alkali dosages per cubic meter of AAS concrete was compensated for by the aggregate content. In dynamic flows, clusters formed near precursor particles may break apart due to the inertial forces from aggregates, particularly when grain sizes exceed 8 mm (Feys et al., 2009). As a result, low-Ms mixtures with higher aggregate content show reduced shear thickening compared to those with higher Ms values.

4. Conclusions

The emphasis of this paper is to evaluate flowability and non-linear rheological characteristics of alkali-activated slag (AAS) concrete. Effects of the activator composition have been studied by varying the activator composition, i.e. the silicate modulus (Ms) and Na_2O content. Structural build-up and workability retention have been investigated as well to further assess the flow properties of AAS concrete. Based on the results of this study, the following conclusions can be drawn.

- Dynamic rheological parameters (yield stress and plastic viscosity) of AAS concrete significantly declined with higher Ms and Na_2O contents in the activator. It has been found in a few mixtures the viscosity was overestimated, while the yield stress might be underestimated by applying the Bingham model due to the non-linearity.
- The Herschel-Bulkley model demonstrated superior accuracy in capturing the rheological behavior of AAS concrete compared to the Bingham model, especially as the shear thinning/thickening became more pronounced due to the variation of activators. However, both models have resulted in similar fitting performance with nearly identical rheological parameters in several linearly behaved mixtures.
- A transition from shear thinning to shear thickening has been observed by increasing Ms in the activator. Shear thinning was detected in low-Ms mixtures, whereas the shear thickening became more evident with higher Ms values and Na_2O content.
- AAS concretes with a lower Ms were characterized with a more rapid build-up process, due to the strong early reactivity. Meanwhile, the build-up rate in the first hour was reduced as Ms and Na_2O content increased, leading to better workability retention.
- This study revealed an exponential relationship between the static yield stress and the slump values of AAS concrete. It is indicated that the yield stress could be estimated through the slump test.

CRediT authorship contribution statement

Jian Zhang: Writing – original draft, Methodology, Investigation, Funding acquisition. **Zhenming Li:** Writing – review & editing, Funding acquisition. **Wentao Wang:** Writing – review & editing, Investigation. **Yaxin Tao:** Writing – original draft, Methodology, Investigation. **Yubo Sun:** Writing – review & editing, Methodology, Investigation, Conceptualization. **Xiangsheng Chen:** Writing – review & editing, Investigation.

Declaration of competing interest

The authors declare that they have no known competing financial interests or personal relationships that could have appeared to influence the work reported in this paper.

Acknowledgments

The authors would like to acknowledge the financial support of National Natural Science Foundation of China (No. 52408279), Major Program of National Natural Science Foundation of China (No. 52090084), the State Key Program of National Natural Science Foundation of China (Grant No. 51938008), Guangdong Provincial Key Laboratory of Intelligent and Resilient Structures for Civil Engineering (No. 2023B1212010004) and State Key Laboratory of High Performance Civil Engineering Materials (No. 2023CEM009). The authors extend their gratitude to Mrs. Zhongqiao Li from Shiyanjia Lab (www.shiyanjia.com) for providing invaluable assistance with the rheological analysis.

Data availability

Data will be made available on request.

References

Alnahhal, M.F., Kim, T., Hajimohammadi, A., 2021. Distinctive rheological and temporal viscoelastic behaviour of alkali-activated fly ash/slag pastes: a comparative study with cement paste. Cement Concr. Res. 144, 106441. https://doi.org/10.1016/j.cemconres.2021.106441.

Alonso, M.M., Gismera, S., Blanco, M.T., Lanzón, M., Puertas, F., 2017. Alkali-activated mortars: workability and rheological behaviour. Constr. Build. Mater. 145, 576–587. https://doi.org/10.1016/j.conbuildmat.2017.04.020.

Alrefaei, Y., Wang, Y.S., Dai, J.G., Xu, Q.F., 2020. Effect of superplasticizers on properties of one-part Ca(OH)2/Na2SO4 activated geopolymer pastes. Constr. Build. Mater. 241, 117990. https://doi.org/10.1016/j.conbuildmat.2019.117990.

Aydın, S., Baradan, B., 2014. Effect of activator type and content on properties of alkali-activated slag mortars. Compos. Part B Eng. 57, 166–172.

Barnes, H.A., 1989. Shear-thickening ("Dilatancy") in suspensions of nonaggregating solid particles dispersed in Newtonian liquids. J. Rheol. (N. Y. N. Y). 33, 329–366.

Criado, M., Palomo, A., Fernández-Jiménez, A., Banfill, P.F.G., 2009. Alkali activated fly ash: effect of admixtures on paste rheology. Rheol. Acta 48, 447–455. https://doi.org/10.1007/s00397-008-0345-5.

Dai, X., Aydin, S., Yardimci, M.Y., Lesage, K., De Schutter, G., 2022. Early age reaction, rheological properties and pore solution chemistry of NaOH-activated slag mixtures. Cem. Concr. Compos. 133, 104715.

De Larrard, F., Ferraris, C.F., Sedran, T., 1998. Fresh concrete: a Herschel-Bulkley material. Mater. Struct. 31, 494–498.

De Schutter, G., Bartos, P.J.M., Domone, P., Gibbs, J., 2008. Self-compacting Concrete. Whittles Publishing, Caithness.

Domone, P.L.J., Yongmo, X., Banfill, P.F.G., 1999. Developments of the two-point workability test for high-performance concrete. Mag. Concr. Res. 51, 171–179. https://doi.org/10.1680/macr.1999.51.3.171.

Duxson, P., Brice, D.G., 2010. Chemical research and climate change as drivers in the commercial adoption of alkali activated materials, 145–155. https://doi.org/10.1007/s12649-010-9015-9.

Egres, R.G., Wagner, N.J., 2005. The rheology and microstructure of acicular precipitated calcium carbonate colloidal suspensions through the shear thickening transition. J. Rheol. (N. Y. N. Y). 49, 719–746.

Favier, A., Hot, J., Habert, G., Roussel, N., D'Espinose De Lacaillerie, J.B., 2014. Flow properties of MK-based geopolymer pastes. A comparative study with standard Portland cement pastes. Soft Matter 10, 1134–1141. https://doi.org/10.1039/c3sm51889b.

Ferraris, C.F., De Larrard, F., 1998. Modified slump test to measure rheological parameters of fresh concrete. Cem. Concr. Aggregates 20, 241–247. https://doi.org/10.1520/cca10417j.

Feys, D., Verhoeven, R., De Schutter, G., 2007. Evaluation of time independent rheological models applicable to fresh self-compacting concrete. Appl. Rheol. 17, 56241–56244.

Feys, D., Verhoeven, R., De Schutter, G., 2008. Fresh self compacting concrete, a shear thickening material. Cement Concr. Res. 38, 920–929. https://doi.org/10.1016/j.cemconres.2008.02.008.

Feys, D., Verhoeven, R., De Schutter, G., 2009. Why is fresh self-compacting concrete shear thickening? Cement Concr. Res. 39, 510–523. https://doi.org/10.1016/j.cemconres.2009.03.004.

Feys, D., Wallevik, J.E., Yahia, A., Khayat, K.H., Wallevik, O.H., 2013. Extension of the Reiner-Riwlin equation to determine modified Bingham parameters measured in coaxial cylinders rheometers. Mater. Struct. Constr. 46, 289–311. https://doi.org/10.1617/s11527-012-9902-6.

Gebregziabiher, B.S., Thomas, R., Peethamparan, S., 2015. Very early-age reaction kinetics and microstructural development in alkali-activated slag. Cem. Concr. Compos. 55, 91–102. https://doi.org/10.1016/j.cemconcomp.2014.09.001.

Gong, M., Li, M., Wang, W., Tan, Z., Sun, Y., 2024. Investigation of micromechanics and relaxation spectrum evolution in multiple recycled asphalt binders. Mater. Struct. 57, 1–18.

Heirman, G., Vandewalle, L., Van Gemert, D., Wallevik, Ó., 2008. Integration approach of the Couette inverse problem of powder type self-compacting concrete in a wide-gap concentric cylinder rheometer. J. Nonnewton. Fluid Mech. 150, 93–103. https://doi.org/10.1016/j.jnnfm.2007.10.003.

Houst, Y.F., Bowen, P., Perche, F., Kauppi, A., Borget, P., Galmiche, L., Le Meins, J.-F., Lafuma, F., Flatt, R.J., Schober, I., 2008. Design and function of novel superplasticizers for more durable high performance concrete (superplast project). Cement Concr. Res. 38, 1197–1209.

Hubler, M.H., Thomas, J.J., Jennings, H.M., 2011. Influence of nucleation seeding on the hydration kinetics and compressive strength of alkali activated slag paste. Cement Concr. Res. 41, 842–846. https://doi.org/10.1016/j.cemconres.2011.04.002.

Juenger, M.C.G., Winnefeld, F., Provis, J.L., Ideker, J.H., 2011. Advances in alternative cementitious binders. Cement Concr. Res. 41, 1232–1243. https://doi.org/10.1016/j.cemconres.2010.11.012.

Koehler, E.P., Fowler, D.W., 2004. Development of a Portable Rheometer for Fresh Portland Cement Concrete.

Krivenko, P., 2017. Why alkaline activation - 60 years of the theory and practice of alkali-activated materials. J. Ceram. Sci. Technol. 8, 323–333. https://doi.org/10.4416/JCST2017-00042.

Laskar, A.I., Bhattacharjee, R., 2011. Rheology of fly-ash-based geopolymer concrete. ACI Mater. J. 108.

Luukkonen, T., Abdollahnejad, Z., Yliniemi, J., Kinnunen, P., Illikainen, M., 2018. One-part alkali-activated materials: a review. Cement Concr. Res. 103, 21–34. https://doi.org/10.1016/j.cemconres.2017.10.001.

Ma, Y., Jin, M., Wang, F., Jacques, D., Shen, X., Zhang, J., Liu, J., 2025. Heating-induced transformations in calcium silicate hydrate (CSH): In-situ investigations of composition, structure, and morphology. Cement Concr. Res. 190, 107819. https://doi.org/10.1016/j.cemconres.2025.107819.

Maranzano, B.J., Wagner, N.J., 2001a. The effects of particle size on reversible shear thickening of concentrated colloidal dispersions. J. Chem. Phys. 114, 10514–10527.

Maranzano, B.J., Wagner, N.J., 2001b. The effects of interparticle interactions and particle size on reversible shear thickening: hard-sphere colloidal dispersions. J. Rheol. (N. Y. N. Y). 45, 1205–1222.

Melrose, J.R., Ball, R.C., 2004a. "Contact networks" in continuously shear thickening colloids. J. Rheol. (N. Y. N. Y). 48, 961–978.

Melrose, J.R., Ball, R.C., 2004b. Continuous shear thickening transitions in model concentrated colloids—the role of interparticle forces. J. Rheol. (N. Y. N. Y). 48, 937–960.

Okamura, H., Ouchi, M., 1999. Self-compacting concrete. Development, present use and future. In: Self-Compacting Concr. Proc. First Int. RILEM Symp. Rilem Publications Cachan Cedex, France, pp. 3–14.

Okamura, H., Ouchi, M., 2003. Self-compacting concrete. J. Adv. Concr. Technol. 1, 5–15.

Palacios, M., Puertas, F., 2011. Effectiveness of mixing time on hardened properties of waterglass-activated slag pastes and mortars. ACI Mater. J. 108, 73.

Palacios, M., Banfill, P.F.G., Puertas, F., 2008. Rheology and setting of alkali-activated slag pastes and mortars: effect of organic admixture. ACI Mater. J. 105, 140.

Palacios, M., Gismera, S., Alonso, M.M., Espinose, J.B., Lacaillerie, D., Lothenbach, B., Favier, A., Brumaud, C., Puertas, F., 2021. Cement and Concrete Research Early reactivity of sodium silicate-activated slag pastes and its impact on rheological properties. Cement Concr. Res. 140, 106302. https://doi.org/10.1016/j.cemconres.2020.106302.

Provis, J.L., 2014. Geopolymers and other alkali activated materials: why, how, and what? Mater. Struct. Constr. 47, 11–25. https://doi.org/10.1617/s11527-013-0211-5.

Provis, J.L., Van Deventer, J.S.J., 2013. Alkali Activated Materials: State-Of-The-Art Report, RILEM TC 224-AAM. Springer Science & Business Media.

Puertas, F., Varga, C., Alonso, M.M., 2014. Rheology of alkali-activated slag pastes. Effect of the nature and concentration of the activating solution. Cem. Concr. Compos. 53, 279–288. https://doi.org/10.1016/j.cemconcomp.2014.07.012.

Puertas, F., González-Fonteboa, B., González-Taboada, I., Alonso, M.M., Torres-Carrasco, M., Rojo, G., Martínez-Abella, F., 2018. Alkali-activated slag concrete: fresh and hardened behaviour. Cem. Concr. Compos. https://doi.org/10.1016/j.cemconcomp.2017.10.003.

Rastogi, S.R., Wagner, N.J., Lustig, S.R., 1996. Rheology, self-diffusion, and microstructure of charged colloids under simple shear by massively parallel nonequilibrium Brownian dynamics. J. Chem. Phys. 104, 9234–9248.

Ren, F., Zhang, J., Yang, J., Chen, X., 2025. Capillary water absorption into alkali-activated slag materials: Experimental and numerical investigation. Dev. Built Environ. 21, 100597. https://doi.org/10.1016/j.dibe.2024.100597.

Ruiz-Sánchez, A., Sánchez-Polo, M., Rozalen, M., 2019. Waste marble dust: an interesting residue to produce cement. Constr. Build. Mater. 224, 99–108.

Sivakrishna, A., Adesina, A., Awoyera, P.O., Kumar, K.R., 2020. Green concrete: a review of recent developments, Mater. Today Proc. 27, 54–58. https://doi.org/10.1016/j.matpr.2019.08.202.

Sun, Y., Ghorbani, S., Dai, X., Ye, G., De Schutter, G., 2022a. Evaluation of rheology and strength development of alkali-activated slag with different silicates sources. Cem. Concr. Compos., 104415

Sun, Y., Zhang, S., Rahul, A.V., Tao, Y., Van Bockstaele, F., Dewettinck, K., Ye, G., De Schutter, G., 2022b. Rheology of alkali-activated slag pastes: new insight from microstructural investigations by cryo-SEM. Cement Concr. Res. 157, 106806. https://doi.org/10.1016/j.cemconres.2022.106806.

Sun, Y., Tao, Y., Rahul, A.V., Ye, G., De Schutter, G., 2022c. Effect of high-range water-reducing admixtures on alkali-activated slag concrete. ACI Mater. J. https://doi.org/10.14359/51737192.

Sun, Y., Miranda, L., Lima, D., Rossi, L., Jiao, D., Li, Z., Ye, G., De Schutter, G., 2023. Cement and Concrete Research Interpretation of the early stiffening process in alkali-

activated slag pastes. Cement Concr. Res. 167, 107118. https://doi.org/10.1016/j.cemconres.2023.107118.
Sun, Y., Mohan, M.K., Dai, X., Zhang, Y., Ye, G., De Schutter, G., 2024a. Effects of mixing conditions and activator anionic species on the rheology of silicate-activated slag concrete. Cem. Concr. Compos. 150, 105556.
Sun, Y., Mohan, M.K., Tao, Y., Zhang, Y., Van Tittelboom, K., Ye, G., De Schutter, G., 2024b. A conceptual design of two-stream alkali-activated materials. Cem. Concr. Compos. 148, 105485. https://doi.org/10.1016/j.cemconcomp.2024.105485.
Tattersall, G.H., Banfill, P.F.G., 1983. The Rheology of Fresh Concrete.
Thwe, E., Khatiwada, D., Gasparatos, A., 2021. Life cycle assessment of a cement plant in Naypyitaw, Myanmar, Clean. Environ. Syst. 2, 100007.
Tsiropoulos, I., Nijs, W., Tarvydas, D., Ruiz, P., 2020. Towards net-zero emissions in the EU energy system by 2050, Insights from Scenar. Line with 2030 2050 Ambitions Eur. Green Deal.
van Deventer, J.S.J., White, C.E., Myers, R.J., 2021. A roadmap for production of cement and concrete with low-CO2 emissions. Waste and Biomass Valorization 12, 4745–4775.
Vieira, L.C., Longo, M., Mura, M., 2021. Are the European manufacturing and energy sectors on track for achieving net-zero emissions in 2050? An empirical analysis. Energy Policy 156, 112464.
Wang, S.D., Scrivener, K.L., Pratt, P.L., 1994. Factors affecting the strength of alkali-activated slag. Cement Concr. Res. 24, 1033–1043. https://doi.org/10.1016/0008-8846(94)90026-4.
Wang, W., Cheng, H., Sun, L., Sun, Y., Liu, N., 2022. Multi-performance evaluation of recycled warm-mix asphalt mixtures with high reclaimed asphalt pavement contents. J. Clean. Prod. 377, 134209.
Wang, X., Yin, Z.-Y., Wu, W., Zhu, H.-H., 2025. Neural network-augmented differentiable finite element method for boundary value problems. Int. J. Mech. Sci. 285, 109783.
Yahia, A., 2011. Cement and Concrete Research Shear-thickening behavior of high-performance cement grouts — in fl uencing mix-design parameters. Cement Concr. Res. 41, 230–235. https://doi.org/10.1016/j.cemconres.2010.11.004.
Yang, B., Jiang, J., Leng, Z., Jiang, X., Sun, Y., Yan, C., Li, G., 2025. Maintenance mechanisms of rejuvenator-optimized asphalt emulsion in damaged porous asphalt mixture: Morphological, physicochemical, and rheological characterizations. Constr. Build. Mater. 464, 140185. https://doi.org/10.1016/j.conbuildmat.2025.140185.
Zhang, J., Ma, Y., Liu, Y., Lai, H., **e, C., Wang, Y., Wang, F., 2025. Investigating dynamic rupture behavior of UHPC-granite interface under impact loading. Theor. Appl. Fract. Mech. 136, 104821. https://doi.org/10.1016/j.tafmec.2024.104821.
Zhang, J., Ma, Y., Zhao, H., Liu, J., Hu, Z., Li, H., Wang, K., Wu, L., 2022. Effect of a novel shrinkage-reducing polycarboxylate superplasticiser on plastic shrinkage cracking of mortars. Mag. Concr. Res. 74, 572–581.
Zhang, J., Ma, Y., Huang, J., Zeng, H., Liu, Z., Hua, T., Liu, J., Hu, Z., 2023. Influence of novel shrinkage-reducing polycarboxylate superplasticizer on the nature of calcium–silicate–hydrates. J. Am. Ceram. Soc. 106, 2139–2154.
Zhang, J., Ma, Y., Liu, J., Chen, X., Ren, F., Chen, W., Cui, H., 2024a. Improvement of shrinkage resistance and mechanical property of cement-fly ash-slag ternary blends by shrinkage-reducing polycarboxylate superplasticizer. J. Clean. Prod. 447, 141493.
Zhang, X., Sun, Y., Zhang, Q., Tian, W., Khan, E., Tsang, D.C.W., 2024b. Leaching characteristics of nutrients in food waste digestate-derived biochar. Bioresour. Technol. 399, 130634.